Structural evaluation and mechanical properties of AZ31/SiC nano-composite produced by FSW process at various welding speeds

A. Abdollahzadeh[1, 3, *], A. Shokuhfar[1], H. Omidvar[2, ×], J.M. Cabrera[3], A. Solonin[4], A. Ostovari[1], M. Abbasi[5]

1- Advanced Materials and Nanotechnology Research Laboratory, Faculty of Materials Science and Engineering, K. N. Toosi University of Technology, Tehran, Iran
2- Faculty of Mining and Metallurgical Engineering, Amirkabir University of Technology, Tehran, Iran
3- Department of Materials Science and Metallurgical Engineering, ETSEIB, Polytechnic University of Catalonia, Barcelona, Spain
4- National University of Science & Technology (MISIS), Moscow, Russian Federation
5- Faculty of Engineering, University of Kashan, Kashan, Iran

× Corresponding author: omidvar@aut.ac.ir
* Co-corresponding author: aabdollahzadeh@mail.kntu.ac.ir

Abstract

A metal matrix composite made of AZ31 containing SiC nano-particles was successfully produced by Friction Stir Welding (FSW) and the effect of processing parameters such as rotational and transversal speeds on the microstructure (grain size) and mechanical properties (tensile and hardness tests) were investigated. Prior to FSW, nano-sized SiC particles were incorporated into the joint line and then different rotational (600, 800 and 1000 rpm) and transversal speeds (25, 75, 125 and 175 mm/min) were tested. Results indicated that the grain size of the matrix and SiC nano-particles are two key parameters controlling different characteristics of the developed composite. Both parameters, in turns, are dependent on the heat generated during the FSW process. The increase of rotational speed and decrease of transversal speed result in high amount of heat and homogeneous distribution of SiC nano-particles. The former leads to grain growth and decrease of strength and hardness while the latter causes grain

refinement and increases of strength and hardness. Accordingly, the heat input has opposite effects on matrix grain growth and homogeneous distribution of particles. Therefore, optimum values of rotational and transversal speeds were found (800 rpm and 75 mm/min) to produce the best microstructure and mechanical properties.

Keywords: Friction stir welding, SiC nano-particles, Mechanical properties, Microstructure, AZ31 magnesium alloy.

1. Introduction

Magnesium alloys have attracted extensive attention as a structural material to be used in aerospace, automobile and other industries [1-2]. Thanks to a combination of unique properties, namely low specific gravity, high specific strength, and high recyclability, magnesium alloys have been of growing importance in industry [3-5]. However, the poor weldability of magnesium alloys is one of its main drawbacks for structural applications. Porosity, hot cracking and segregation have been reported as the main defects associated to welding of magnesium alloys [6-8].

On the other hand, magnesium alloys display relatively low absolute yield stresses. In order to overcome this problem, many researchers investigate the effect of reinforcing with second phase particles. Different ways have been proposed to obtain this kind of metal matrix composite. Friction Stir Welding (FSW) and Friction Stir Processing (FSP) [9] are among these methods. Indeed, FSW and FSP processes are very similar, but the former is used for joining two plates and the latter is applied for surface processing of one single plate. During FSW and FSP processes, a non-consumable rotating tool is inserted into the abutting edges of sheets or plates to be joined and moved at a constant rate along the joint line [9]. Accordingly, heat is generated between tool and material which leads to a very soft region near the tool. The tool then mechanically “stir” the pieces of metal at the contact place.

Recently, many researchers utilized FSP to produce magnesium matrix composites by addition of micro and nano-particles in the stir zone. But, joining and simultaneous nano-composite fabrication in magnesium alloys using FSW method has been rarely investigated [10-11].

During FSP, the material in the stirred zone experience severe plastic deformation. The material flow produced by stirring and severe plastic deformation can be used for modification of bulk alloy due to mixing of second element. This mixing is followed by distribution of fine particles of the second element, the precipitation of a second phase, increased density of defects, and so forth. Finally, the stirred zone becomes a metal matrix composite with an enhanced wear resistance and hardness [12].

Abbasi et al. [13] studied the effect of FSP on the tribological and corrosion behavior of a magnesium AZ91 alloy. During stirring, they added hard particles, namely SiC and Al_2O_3, to the stir zone. The results indicated that wear and corrosion resistance of FSPed samples were higher than the as-received material. Their results also showed that the samples processed by SiC particles had better mechanical characteristics and corrosion resistance than the samples processed by Al_2O_3 particles.

Karthikeyan and Mahadevan [14] investigated the effects of SiC particles addition in the weld zone during FSW of an Al 6351 alloy. Their results revealed that the mechanical properties of welded metal matrix joints were better than those of the plain Al 6351 alloy. They argued that a pining effect of the SiC particles restricted the grain growth during the process.

Lately, Sun and Fujii [15] applied SiC particles along the joint line to produce a copper matrix composite in the stir zone (SZ). Using a square pin tool, they noticed that single-pass processed specimen fractured preferentially in the zone where reinforcements was greatly aggregated. Finally, Bahrami et al. [16] successfully welded 7075 aluminum alloy plates while SiC nano-particles were introduced into the weld line. They pointed out that SiC reinforcement play a crucial role in the overall mechanical properties of the joints. They showed that high rotational speed promoted interesting results. For instance, at 1250 rpm (rotational speed) and 40 mm/min (transversal speed), they observed 31 % increase in ultimate tensile strength (UTS) as well as 76.1 % enhancement in elongation of the weldments associated to the addition of SiC nano-particles. Moreover, they conducted other research on the effect of pin geometry and found promising results with threaded taper pin tool [17-18].

In the present communication , the effects of rotational and transversal speeds on grain size, tensile properties and hardness of an AZ31 matrix composite containing SiC particles were investigated. The composite was fabricated via the FSW method.

2. Experimental procedure

Fully annealed AZ31 magnesium alloy plate with dimensions of 200×155×6 mm and SiC nano-particles with mean particles size of 45-65 nm were used as parent metal and reinforcements, respectively. Table 1 shows the chemical composition of the studied magnesium alloy. Initially a groove on the contacting surface of two adjoining plates was designed to make home for SiC particles. Specimens were welded by using the FSW technique, while three rotational speeds of 600, 800 and 1000 rpm, and four transversal speeds of 25, 75, 125 and 175 mm/min were carried out. The different welding condition for all experiments are shown in Table 2. The tilt angle was

2 degrees in all the experiments. The FSW tool used in this process was fabricated from H13 tool steel rod. Tool details are provided in Table 3.

Optical and scanning electron microscopes along with ImageJ software were employed to examine the microstructural evolutions and measure the grain size. For this purpose metallographic specimens were prepared according to ASTM-E3 [19] and then etched for 1–2 s using an etching solution consisting of 4.2 g picric acid, 10 ml acetic acid, 10 ml water, and 70 ml ethanol.

Hardness of the stir zone was evaluated using micro-hardness measurement employing a Vickers indenter with a load of 25 N for a dwell time of 10 s. Reported hardness values are mean value of 5 readings. Indentations were done at a distance of 1 mm from each other. Subsize tensile test samples according to ASTM-E8 standard test [20] were machined to derive the mechanical properties. The samples were obtained from the welded specimens using wire cut method in a way that the weld was positioned in the middle of the gauge section. During the tensile test, the strain rate was 5 mm/min.

3. Results and discussion

3.1. Structure

Fig 1. depicts the macrostructure of some samples processed at various welding conditions. Non-homogeneous distribution of reinforcing particles, presence of voids and incomplete stirring of material in the weld zone are some of the problems that can be noticed in Figs 1a, 1b and 1c, respectively, and they might occur during FSW while reinforcing particles are incorporated. Proper welding conditions inhibit the occurrence of the above mentioned problems and a suitable macrostructure is then developed as shown in Fig. 1d.

The grain size of weld zone has a significant influence on the mechanical properties of the weld such as tensile strength, toughness properties, hardness and plasticity. Thus, fine-grained structure could improve these properties. It is widely known that Dynamic recrystallization (DRX) during FSW will cause the formation of fine equiaxed grains in the stir zone, and process parameters is one of the most important factors affecting the microstructure and grain size of the weld [12].

To investigate these effects, different microstructures resulting from various welding conditions are also presented in Fig. 2 and also dependence of the grain size against the transversal and rotational speeds is presented in Fig. 3.

As a general trend, one can see that at a constant value of rotational speed, grain size decreases as transversal speed increases. This trend fails when considering the highest transversal speed tested. Furthermore, it can be observed from Fig. 3a that there is a minimum (optimal) grain size at a given rotational speed. Variation of the rotational speed around the optimum value promotes larger grain sizes. This fact can be explained in terms of the balance between the heat generated during FSW and the presence of SiC particles as reinforcement particles which hinder the movement of dislocations and the grain boundaries.

On the other hand, it is recognized in the literature that low transversal speed and high rotational speed during FSW is one of the primary reasons for high heat generation in the weld zone [21]. It is also known that this heat generation promotes grain growth (whether in the welded zone or in the heat affected area) and therefore softens the alloy. Very high degree of softening results in more complete stirring of material, but, on the contrary, it can lead to more homogeneous distribution of SiC particles [22]. Indeed, small SiC particles with narrow range of particles size distributed in all areas of the stir zone are consequences of homogeneous distribution of particles. It appears from scanning electron microscopy (SEM) images in Fig. 4.

It is known that second phase particles hinder the movement of dislocations and grain boundaries [23]. According to Orowan-Ashby equation [23], this mechanism depends on the size and volume fraction of particles. High volume fraction of small particles has the strongest effect. So, the heat generation have opposite effects on grain size. On one side heat generation promotes grain growth, but on the other side, heat generation favor the homogeneous distribution of the SiC particles, which, in turns, enhances the pinning effect of grain boundaries. The opposite happens when the generated heat is low, in this condition, grain growth cannot take place due to the lack of thermal activation, but a very small volume fraction of particles are distributed in welded zone, so they do not represent obstacles to dislocation motion.

It should be pointed out that all particles depicted in Fig. 4 are not SiC particles. For instance white particle denote (Al, Mn) precipitations. Energy dispersive spectroscopy (EDS) results for points A, B and C are presented in Fig. 5 and the (Al, Mn) precipitates were identified as Al_3Mn.

SEM picture of Al_3Mn phase in higher magnification is shown in Fig. 6. Wavelength-dispersive spectroscopy (WDS) analyses of this particle to trace Al and Mg elements are also depicted in Fig. 7. It is observed that the particle has a dimension of about 14 µm.

Laser et al. indicated that during FSW of AZ31, the maximum temperature achieved is 610 °C [24], which is lower than the melting point of Al_3Mn [25]. Commin et al. inferred that (Al, Mn) precipitates does not dissolve during FSW [26] and they may break into small particles, due to the severe deformation imparted by FSW [9]. The presence of Al_3Mn particles in the microstructure of the stirred zone, as can be seen in Fig. 4 confirms that these particles did not dissolve during FSW. However the particle size in the welded area is lower than those in base metal as illustrated in Fig. 8.

3.2. Mechanical properties

The effects of rotational and transversal speeds on mechanical properties, namely yield and tensile strength and elongation of the current composite are shown in Figs. 9-11, respectively. It is observed that the effect of rotational and transversal speeds on strength and elongation values is not monotonic and a maximum value is obtained in the rotational speed of 800 rpm and transversal speed of 75 mm/min, and this is in line with the obtained grain size. In other words, the higher mechanical properties are obtained when rotational and transversal speeds are set to optimum values. The same can be said regarding the elongation to fracture behavior that it is seen from Fig 11.

It can be found from Figs. 9 to 11 that neither high rotational and low transversal speeds, nor low rotational and high transversal speeds guarantee the highest strength and elongation. This result can be explained by Hall-Petch and Orowan-Ashby equations [23]. According to Hall-Petch equation, strength is dependent to the grain size in the following manner [23]:

$$\sigma = \sigma_i + kD^{-\frac{1}{2}} \qquad (1)$$

where σ_i is a friction stress,

k is material constant parameter and

D is the grain size

On the other hand Orowan-Ashby equation denotes that the strengthening by second-phase particles is related to interparticle spacing as [23]:

$$\Delta\sigma \approx k'\lambda^{-\frac{1}{2}} \qquad (2)$$

where k' is a constant and

λ is the interparticle spacing

According to Equation 1 and 2, when grain size and interparticle spacing are low, the strengthening is high. Additionally, ductility (and therefore elongation) increases as the grain size and interparticle spacing decrease [27]. Therefore, during processing of the current AZ31 Mg metal matrix containing SiC particles, neither a high heat generation (which promotes grain growth) nor low heat generation (which promotes a large interparticle spacing), guarantee the best mechanical properties of the weld.

In addition, low and high heat generation by FSW might have other affects. Mishra et al. [28] pointed out that low heat generation in the weld zone is not enough to soften materials, and in consequence a bad stirring happens in the stir zone. If the material is too cold then voids or other flaws may be present in the stirred zone and in some extreme cases the tool may break because of the high forces acting. Excessively high heat input, on the other hand, may be detrimental to the final properties of the weld, due to the presence of low-melting-point phases and the above mentioned chance to grain growth [28].

Finally, the effect of rotational and transversal speeds on the hardness of developed composite are depicted in Fig. 12. Similarly to the yield strength, there are optimum values for rotational and transversal speeds which result in the highest hardness of developed composite. Both low grain size and distance between the second phase particles result in inhibition of dislocations movement and correspondingly hardness increases such as yield strength or tensile strength [29-30].

Conclusions

In the current research, AZ31 magnesium matrix composite containing SiC particles were produced by FSW, and the effects of rotational and transversal speeds on the microstructure and mechanical properties of the developed composite was investigated. Different rotational and transversal speeds were tested. Yield strength of 131 MPa, tensile strength of 240 MPa, and ductility value of 8.2 percent were obtained for the developed composite while rotational speed of 800 rpm and transversal speed of 75 mm/min were applied. Also, it can be concluded that:

1- The heat generated during FSW is dependent on the welding condition and the combination of transversal and rotational speeds is one of the important parameter affecting the mechanical properties of the developed composite.

2- The heat generated during FSW affects the grain size of metal matrix and the distribution of SiC nano-particles. When the heat generated overpass a given value, grain growth takes place but SiC nano-particles distribute more homogeneously in matrix. On the contrary, when the heat is low, limited grain growth occurs and SiC nano-particles distribute less homogeneously.

3- The low grain size of metal matrix increases the strength, hardness and ductility, while the heterogeneous distribution of SiC nano-particles decreases these properties.

4- The best mechanical properties of fabricated composite is obtained when the welding parameters, rotational and transversal speeds, are set at optimum values.

Table captions:

Table 1. Chemical composition of the current AZ31 magnesium alloy (wt. %).

Table 2. Specimen's code and process conditions.

Table 3. Detailed features of the tool used for FSW.

Figure captions:

Fig. 1 Macrostructure of some processed samples at various welding conditions, a) formation of cavity in the specimen FSWed at 600 rpm and 25 mm/min, b) non-homogeneous distribution of SiC particles in the specimen FSWed at 600 rpm and 75 mm/min, c) incomplete stirring of material in the stir zone of specimen FSWed at 1000 rpm and 25 mm/min, d) fair macrostructure in the specimen FSWed at 800 rpm and 125 mm/min.

Fig. 2 Microstructures of different samples welded using various welding conditions, namely rotational and transversal speed indicated in the upper left corner of each picture.

Fig. 3 The effect of a) rotational and b) transversal speeds on grain size.

Fig. 4 SEM pictures of two FS welded samples, a) the distribution of SiC particles is homogeneous in the specimen FSWed at 800 rpm and 75 mm/min (arrows refer to SiC particles), b) the distribution of SiC particles is non-homogeneous in the specimen FSWed at 600 rpm and 75 mm/min (A and B denote the SiC-rich and SiC-poor regions, respectively and C indicates presence of precipitation).

Fig. 5 EDS peaks of points A, B and C denoted in Fig. 4b, a) SiC-rich region, b) SiC-poor region and c) Al3Mn phase.

Fig. 6 SEM picture of Al3Mn phase at high magnification.

Fig. 7 WDS analyses of Al3Mn phase to trace, a) aluminum and b) magnesium elements.

Fig. 8 Al3Mn precipitates in a) base metal and b) fusion zone.

Fig. 9 The effect of a) rotational and b) transversal speeds on yield strength.

Fig. 10 The effect of a) rotational and b) transversal speeds on tensile strength.

Fig. 11 The effect of a) rotational and b) transversal speeds on elongation.

Fig. 12 The effect of a) rotational and b) transversal speeds on hardness.

References

1- Friedrich H E, Mordike B L. Magnesium Technology: Metallurgy, Design Data, Applications. Springer, Germany 2006.

2- Kainer K U. Magnesium alloys and technologies. WILEY-VCH, Germany 2003.

3- Avedesian M, Baker H. ASM specialty handbook: magnesium and magnesium alloys, ASM International, USA 1999.

4- Zuberova Z, Estrin Y, Lamark T T, Janecek M, Helling R J, Krieger M. Effect of equal channel angular pressing on the deformation behavior of magnesium alloy AZ31 under uniaxial compression. Journal of Materials Processing Technology 2007, 184: 294-299.

5- Alavi Nia A, Omidvar H, Nourbakhsh S H. Investigation of the effects of thread pitch and water cooling action on the mechanical strength and microstructure of friction stir processed AZ31. Materials and Design 2013, 52: 615-620.

6- Czerwinski F. Welding and joining of magnesium alloys, in: Magnesium alloys- design, processing and properties. InTech Publication, Croatia 2011.

7- Liu L, Ren D, Liu F. A review of dissimilar welding technologies for magnesium alloys to aluminum alloys. Materials 2014, 7: 3735-3757.

8- Alavi Nia A, Omidvar H, Nourbakhsh S H. Effects of an overlapping multi-pass friction stir process and rapid cooling on the mechanical properties and microstructure of AZ31 magnesium alloy. Materials and Design 2014, 58: 298-304.

9- Mishra R S, Ma Z Y. Friction stir welding and processing. Materials Science and Engineering R 2005, 50: 1-78.

10- Abdolahzadeh A, Omidvar H, Safarkhanian M A, Bahrami M. Studying microstructure and mechanical properties of SiC-incorporated AZ31 joints fabricated through FSW: the effects of rotational and travelling speeds. Advanced Manufacturing Technology 2014, 75: 1189-1196.

11- Abbasi M, Abdollahzadeh A, Omidvar H, Bagheri B, Rezaei M. Incorporation of SiC particles in FS welded zone of AZ31 Mg alloy to improve the mechanical properties and corrosion resistance. International Journal of Materials Research 2016, 107: 566-572.

12- Heidarzadeh A, Kazemi-Choobi K, Hanifian H, Asadi P. 3-microstructural evolution. In: Besharati-Givi M K, Asadi P (eds). Advances in Friction-Stir Welding and Processing. Woodhead Publishing, 2014, pp. 65–140.

13- Abbasi M, Bagheri B, Dadaei M, Omidvar H, Rezaei M. The effect of FSP on mechanical, tribological, and corrosion behavior of composite layer developed on magnesium AZ91 alloy surface. The International Journal of Advanced Manufacturing Technology 2015, 77: 2051-2058.

14- Karthikeyan P, Mahadevan K. Investigating on the effects of SiC particles addition in the weld zone during friction stir welding of Al 6351 alloy. International Journal of Advanced Manufacturing Technology 2015, 80:

15- Sun Y F, Fujii H. The effect of SiC particles on the microstructure and mechanical properties of friction stir welded pure copper joints. Materials Science and Engineering A 2011, 528: 5470-5475.

16- Bahrami M, Besharati Givi M K. A novel approach to develop aluminum matrix nano-composite employing friction stir welding technique. Materials and Design 2014, 53: 217-225.

17- Bahrami M, Dehghani K, Besharati Givi M K. Exploring the effects of SiC reinforcement incorporation on mechanical properties of friction stir welded 7075 aluminum alloy: Fatigue life, impact energy, tensile strength. Materials Science and Engineering A 2014, 595: 173-178.

18- Bahrami M, Dehghani K, Parvin N On the role of pin geometry in microstructure and mechanical properties of AA7075/SiC nano-composite fabricated by friction stir welding technique. Materials and Design 2014, 53: 519-527.

19- ASTM E3-11, Standard guide for preparation of metallographic specimens, ASTM International, West Conshohocken, PA 2011.

20- ASTM E8 / E8M-15, Standard Test Methods for Tension Testing of Metallic Materials, ASTM International, West Conshohocken, PA 2011.

21- Rafiei R, Ostovari Moghaddam A, Hatami M R, Khodabakhshi F, Abdolahzadeh A, Shokuhfar A. Microstructural characteristics and mechanical properties of the dissimilar friction-stir butt welds between an Al–Mg alloy and A316L stainless steel. The International Journal of Advanced Manufacturing Technology 2016, pp. 1-17.

22- Abbasi M, Abdollahzadeh A, Bagheri B, Omidvar H. The effect of SiC particle addition during FSW on microstructure and mechanical properties of AZ31 magnesium alloy. Journal of Materials Engineering and Performance 2015, 24: 5037-5045.

23- Dieter G E, Bacon D. Mechanical Metallurgy. McGraw-Hill, London 1988.

24- Laser T, Nurnberg M R, Janz A, Hartig C, Leitzig D, Schmid-Fetzer R, et al. The influence of manganese on the microstructure and mechanical properties of AZ31 gravity die cast alloys. Acta Mater 2006, 54: 3033-3041.

25- Perry D L, Handbook of inorganic compounds, CRC Press, USA 2011.

26- Commin L, Dumont M, Masse J E, Barrallier L. Friction stir welding of AZ31 magnesium alloy rolled sheets: influence of processing parameters. Acta Materialia 2009, 57: 326-334.

27- Mukai T, Mohri T, Mabuchi M, Nakamura M, Ishikawa K, Higashi K. Experimental study of a structural magnesium alloy with high absorption energy under dynamic loading. Scripta Materialia 1998, 39: 1249-1253.

28- Mishra R S, De P S, Kumar N. Friction stir welding and processing: science and engineering. Springer, London 2014.

29- Kumar P V, Reddy G M, Rao K S. Microstructure and pitting corrosion of armor grade AA7075 aluminum alloy friction stir weld nugget zone- effect of post weld heat treatment and addition of boron carbide. Defense Technology 2015, 11: 166-173.

30- Huang Y, Wang T, Guo W, Wan L, Lv S. Microstructure and surface mechanical property of AZ31/SiC surface composite fabricated by direct friction stir processing. Materials and Design 2014, 59: 274-278.

Table 1. Chemical composition of the current AZ31 magnesium alloy (wt. %).

Element	Mg	Al	Zn	Mn	Ca	Cu	Fe	Other
Weight percent	95.75	2.82	0.94	0.42	0.023	0.011	0.0045	0.03

Table 2. Specimen's code and process conditions.

Specimen number	Rotation speed(rpm)	Traveling Speed (mm/min)
1	600	25
2	600	75
3	600	125
4	600	175
5	800	25
6	800	75
7	800	125
8	800	175
9	1000	25
10	1000	75
11	1000	125
12	1000	175

Table 3. Detailed features of the tool used for FSW.

characteristics	details
Tools material	H13 steel
Shape of pin	Frustum
Shoulder diameter	20 mm
Big diameter of pin	7.2 mm
Small diameter of pin	5.1 mm
Length of pin	5.8 mm

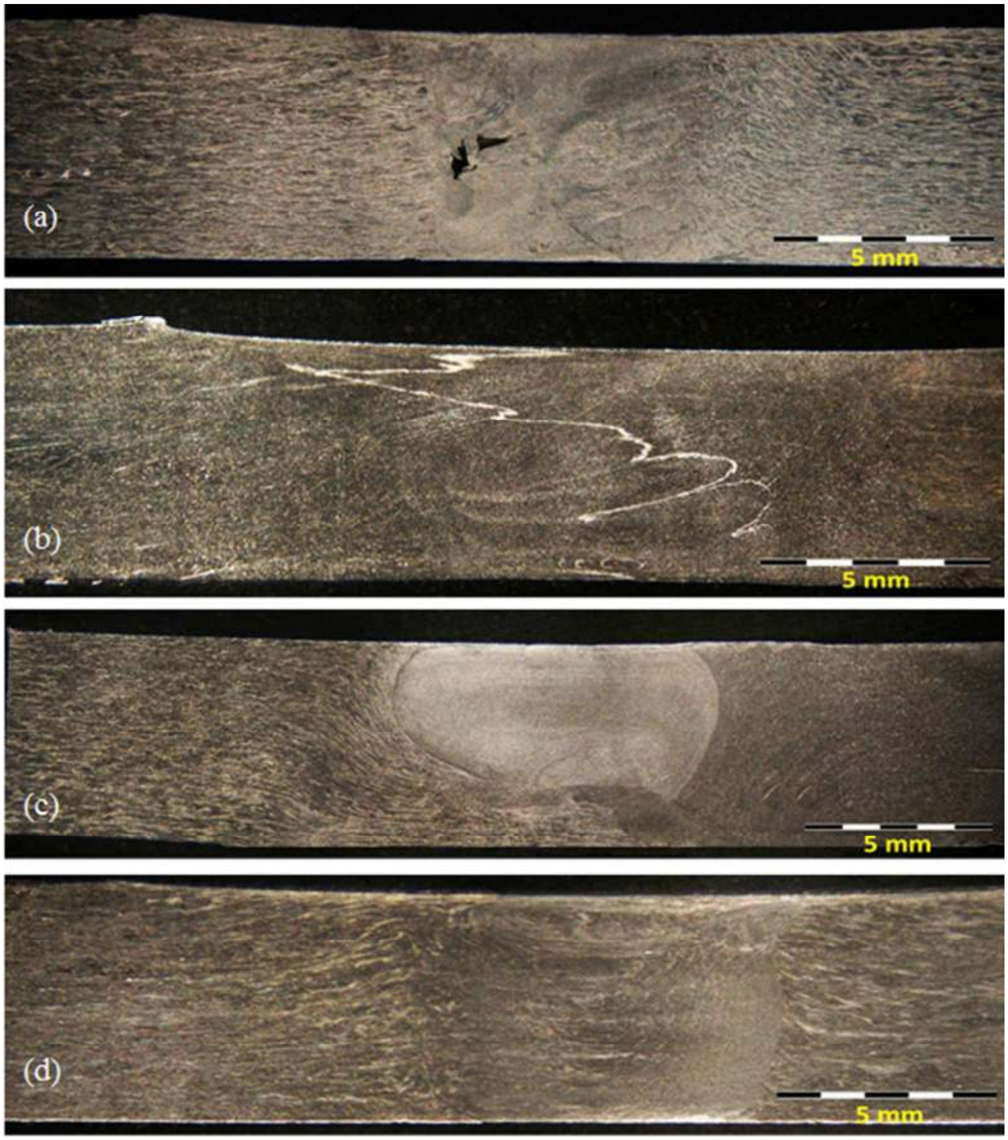

Fig. 1 Macrostructure of some processed samples at various welding conditions, a) formation of cavity in the specimen FSWed at 600 rpm and 25 mm/min, b) non-homogeneous distribution of SiC particles in the specimen FSWed at 600 rpm and 75 mm/min, c) incomplete stirring of material in the stir zone of specimen FSWed at 1000 rpm and 25 mm/min, d) fair macrostructure in the specimen FSWed at 800 rpm and 125 mm/min.

154x176mm (96 x 96 DPI)

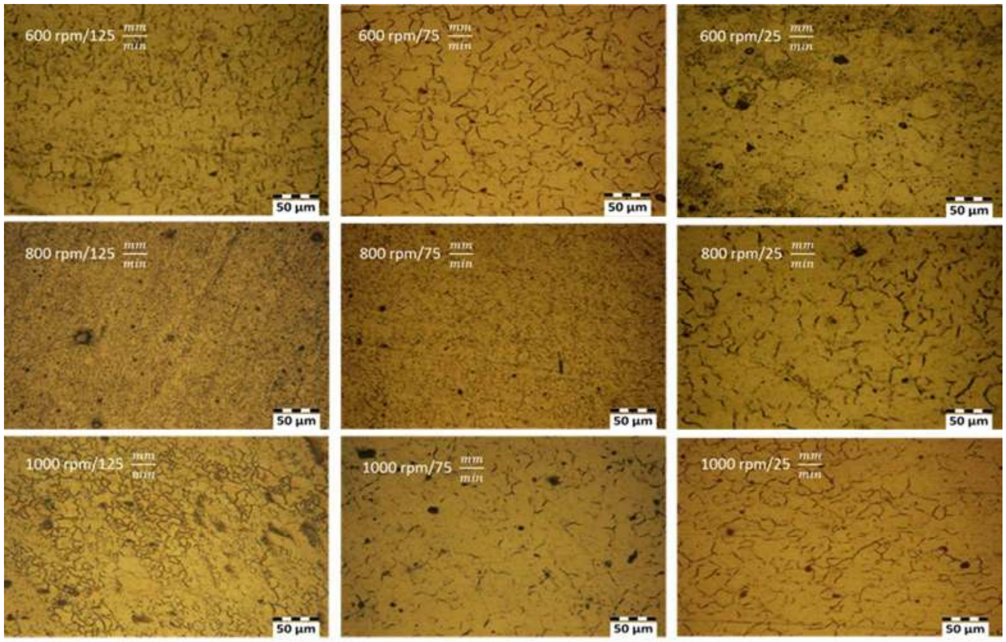

Fig. 2 Microstructures of different samples welded using various welding conditions, namely rotational and transversal speed indicated in the upper left corner of each picture.

233x148mm (96 x 96 DPI)

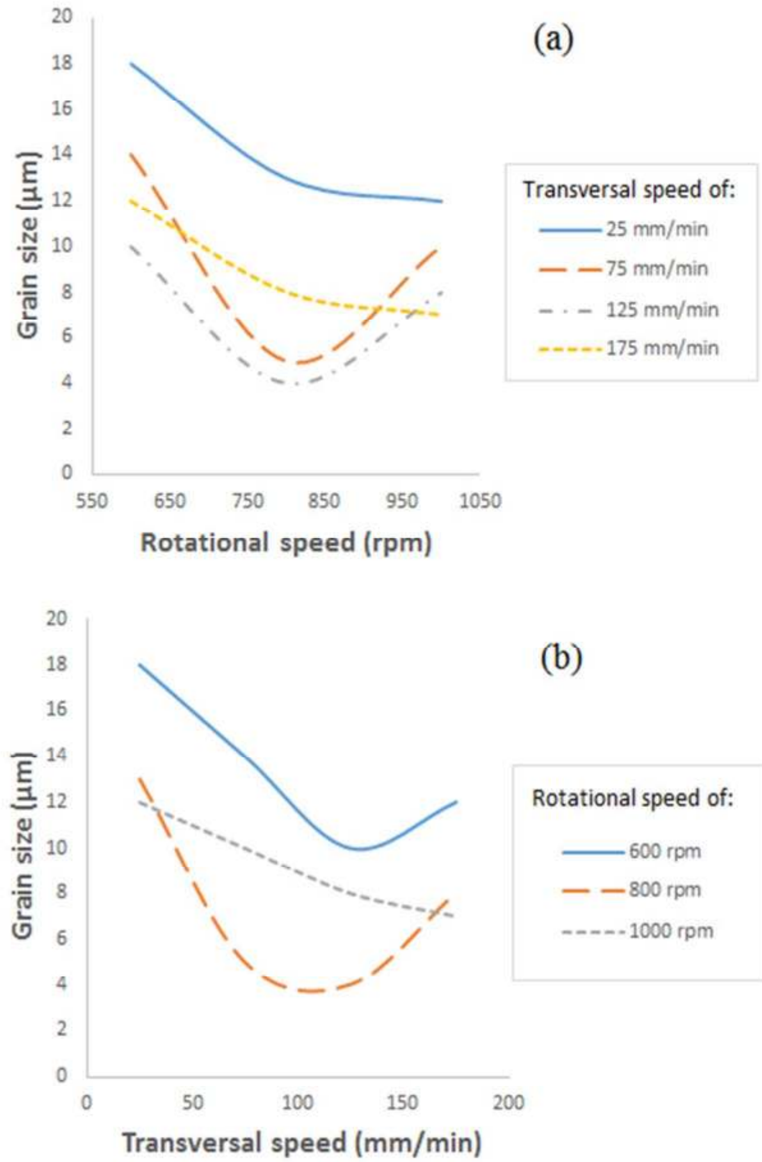

Fig. 3 The effect of a) rotational and b) transversal speeds on grain size.

133x178mm (96 x 96 DPI)

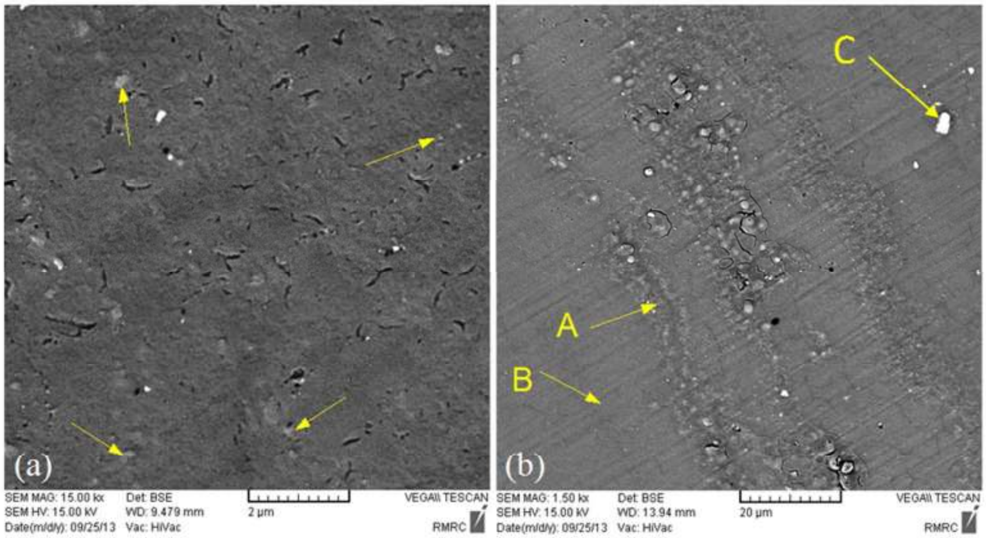

Fig. 4 SEM pictures of two FS welded samples, a) the distribution of SiC particles is homogeneous in the specimen FSWed at 800 rpm and 75 mm/min (arrows refer to SiC particles), b) the distribution of SiC particles is non-homogeneous in the specimen FSWed at 600 rpm and 75 mm/min (A and B denote the SiC-rich and SiC-poor regions, respectively and C indicates presence of precipitation).

247x136mm (96 x 96 DPI)

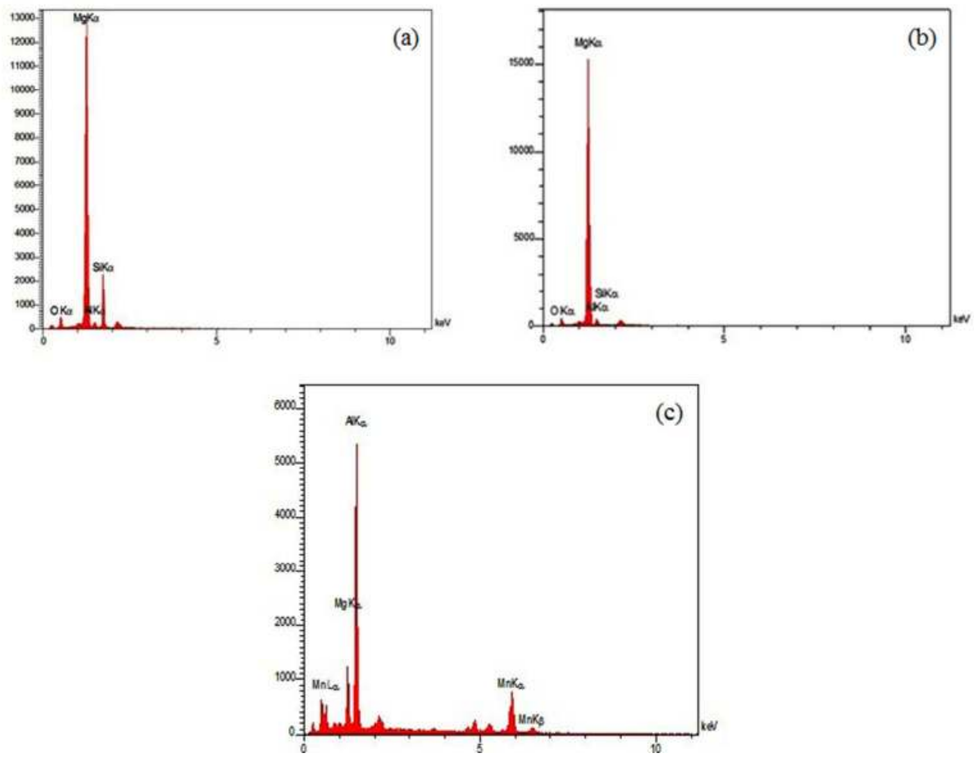

Fig. 5 EDS peaks of points A, B and C denoted in Fig. 4b, a) SiC-rich region, b) SiC-poor region and c) Al3Mn phase.

201x152mm (96 x 96 DPI)

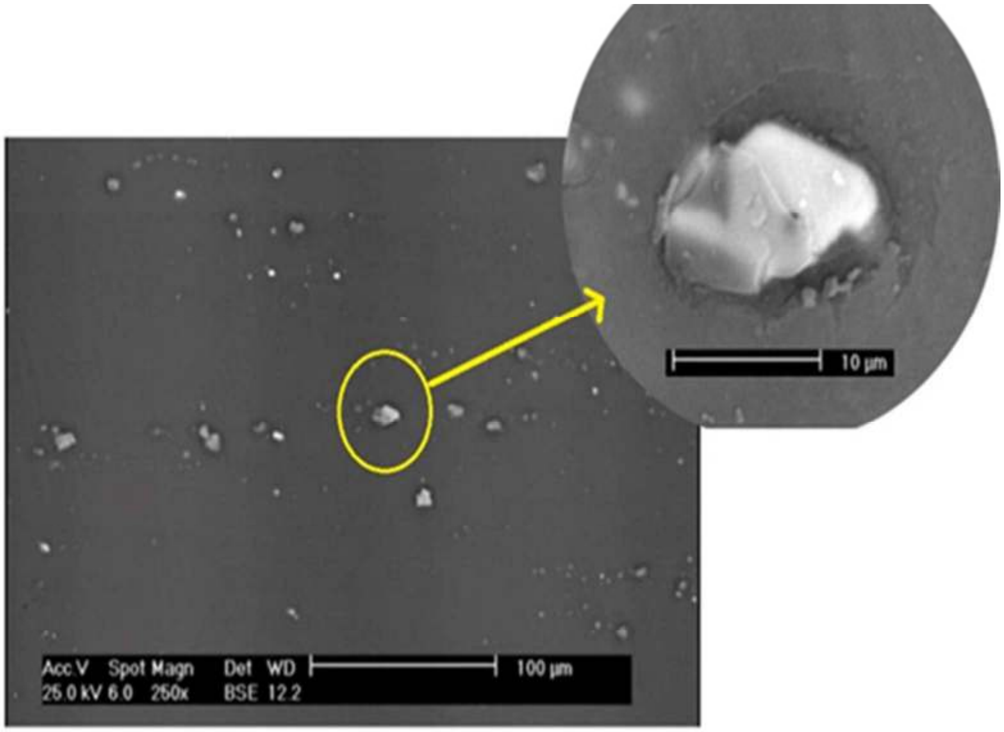

Fig. 6 SEM picture of Al3Mn phase at high magnification.

166x121mm (96 x 96 DPI)

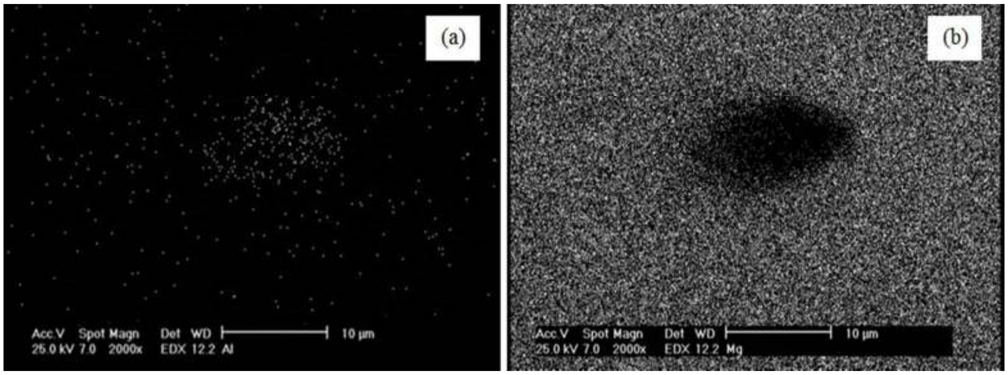

Fig. 7 WDS analyses of Al3Mn phase to trace, a) aluminum and b) magnesium elements.

245x89mm (96 x 96 DPI)

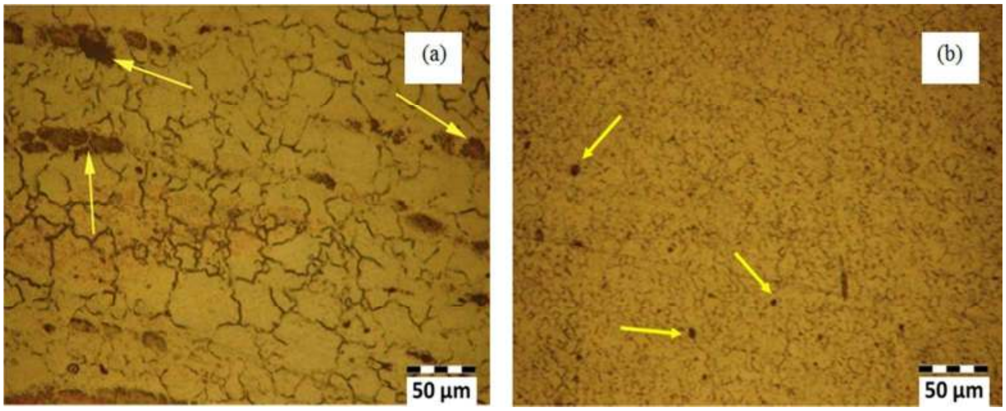

Fig. 8 Al3Mn precipitates in a) base metal and b) fusion zone.

244x98mm (96 x 96 DPI)

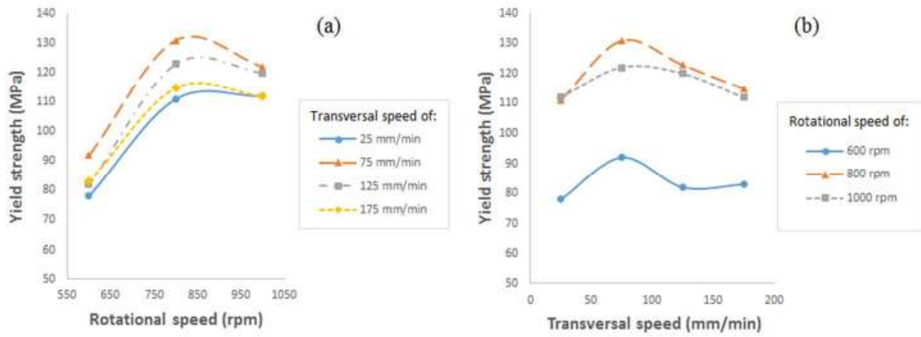

Fig. 9 The effect of a) rotational and b) transversal speeds on yield strength.

251x89mm (96 x 96 DPI)

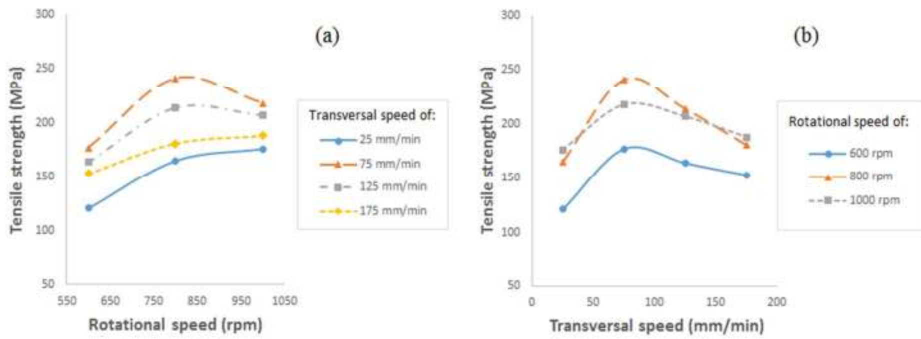

Fig. 10 The effect of a) rotational and b) transversal speeds on tensile strength.

250x89mm (96 x 96 DPI)

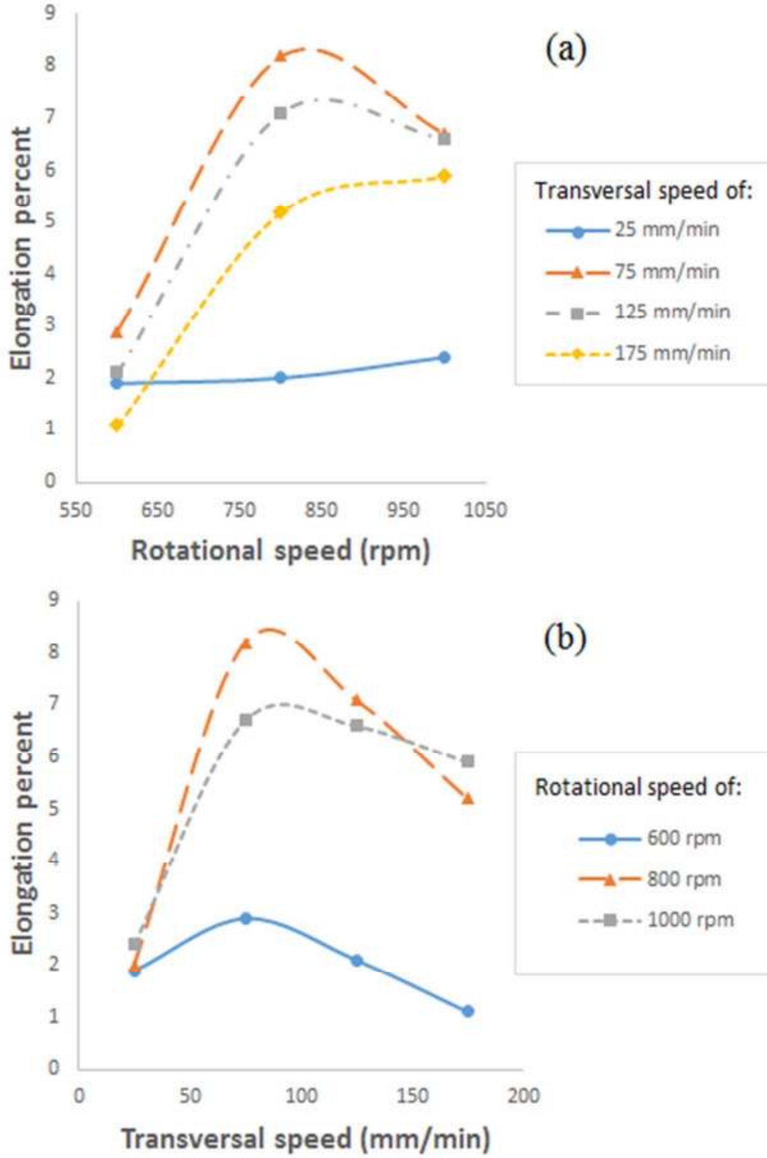

Fig. 11 The effect of a) rotational and b) transversal speeds on elongation.

131x174mm (96 x 96 DPI)

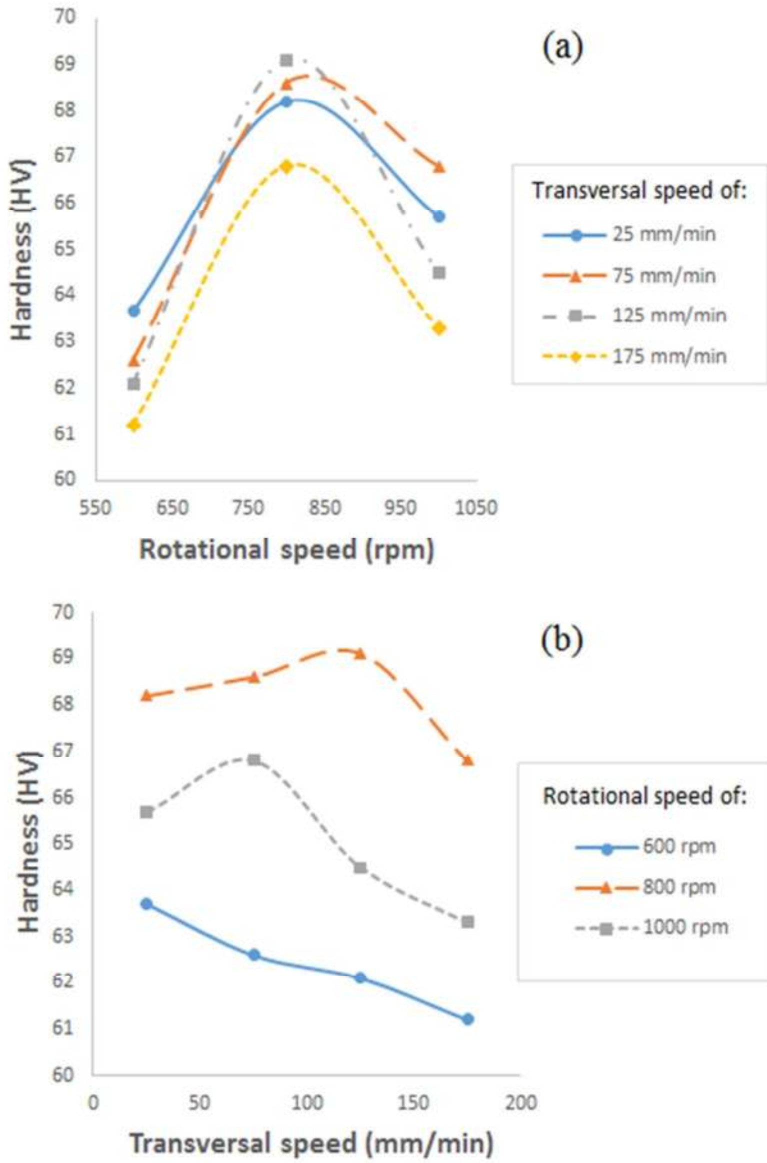

Fig. 12 The effect of a) rotational and b) transversal speeds on hardness.

134x176mm (96 x 96 DPI)